Received: 8 September 2020 | Revised: 21 December 2020 | Accepted: 30 December 2020

DOI: 10.1002/hyp.14033

RESEARCH ARTICLE

WILEY

Improved understanding of dynamic water and mass budgets of high-alpine karst systems obtained from studying a well-defined catchment area

Simon Frank | **Nadine Goeppert** | **Nico Goldscheider**

Institute of Applied Geosciences, Division of Hydrogeology, Karlsruhe Institute of Technology (KIT), Karlsruhe, Germany

Correspondence
Simon Frank, Institute of Applied Geosciences, Division of Hydrogeology, Karlsruhe Institute of Technology (KIT), Kaiserstr. 12, 76131 Karlsruhe, Germany.
Email: simon.frank@kit.edu

Funding information
Bundesministerium für Bildung und Forschung, Grant/Award Number: 01DH19022A; FP7 People: Marie-Curie Actions, Grant/Award Number: 303837

Abstract

Large areas of Europe, especially in the Alps, are covered by carbonate rocks and in many alpine regions, karst springs are important sources for drinking water supply. Because of their high variability and heterogeneity, the understanding of the hydrogeological functioning of karst aquifers is of particular importance for their protection and utilisation. Climate change and heavy rainfall events are major challenges in managing alpine karst aquifers which possess an enormous potential for future drinking water supply. In this study, we present research from a high-alpine karst system in the UNESCO Biosphere Reserve Großes Walsertal in Austria, which has a clearly defined catchment and is drained by only one spring system. Results show that (a) the investigated system is a highly dynamic karst aquifer with distinct reactions to rainfall events in discharge and electrical conductivity; (b) the estimated transient atmospheric CO_2 sink is about 270 t/a; (c) the calculated carbonate rock denudation rate is between 23 and 47 mm/1000a and (d) the rainfall-discharge behaviour and the internal flow dynamics can be successfully simulated using the modelling package KarstMod. The modelling results indicate the relevance of matrix storage in determining the discharge behaviour of the spring, particularly during low-flow periods. This research and the consequent results can contribute and initiate a better understanding and management of alpine karst aquifers considering climate change with more heavy rainfall events and also longer dry periods.

KEYWORDS
CO_2 sink, denudation rate, groundwater, hydrochemical variability, karst spring, rainfall-discharge model

1 | INTRODUCTION

Carbonate rocks, representing potential karst aquifers, cover about 15% of the world's land surface (Goldscheider et al., 2020) and karst water resources are important for the drinking water supply of approximately 750 million people worldwide (Stevanović, 2018). In Austria, 25% of the land surface is covered by carbonate rocks (Chen et al., 2017), but over 50% of the population, including large cities like Vienna, Salzburg, and Innsbruck, depend on drinking water from alpine karst aquifers (Kralik, 2001).

High-alpine karst aquifers offer a high potential for future water supply. Karst aquifers have complex and original characteristics, which make them different from other aquifer types (Bakalowicz, 2005) and often very vulnerable to contamination, especially after rain events, because recharge occurs directly through dolines, fissures or swallow holes. Consequently, karst springs often show strong and rapid variations in discharge and water quality in response to rain events (Pronk et al., 2007).

The complex hydrogeological behaviour of karst aquifers results from the complex interaction of many geological and hydrological variables as the evolving porosity and permeability of carbonate rocks, which are the result of chemical interaction of the carbonate rocks and water flowing through them. The water flow is important for the aquifer development, because this flow serves as primary transport mechanism in the dissolution of carbonate rocks (Petalas et al., 2018).

Several studies have been conducted in order to understand and describe the hydrogeological functioning of karst aquifers and the complex behaviours of karst springs (e.g., Birk et al., 2004; Filippini et al., 2018; Goldscheider, 2005; Linan Baena et al., 2009; Vigna & Banzato, 2015). Because springs in this environment are often directly related to precipitation and recharge in the catchment, especially shallow and fast flow karst systems can be investigated by means of tracer tests and hydrograph and chemograph analysis (Hilberg & Kreuzer, 2013). Another important process, which is often described in the literature (e.g., Frank et al., 2019; Martin & Dean, 2001), is the interaction between karst conduits and the surrounding matrix. This process is important, as the matrix can act as a water storage, particularly during dry periods. Nevertheless, a qualitative and quantitative description of this process is rare. Within this study, this process was studied for the investigated karst system in Austria and its importance during low-flow conditions is shown.

In addition to the already complex behaviour of karst systems, climate change is a challenge in managing such alpine karst aquifers. Climate change scenarios project more heavy rain events in the future but at the same time also more and longer dry periods (Dobler et al., 2013; Rössler et al., 2012). The understanding of the functioning of these complex karst aquifers is important for the utilisation and protection of karst springs, particularly in high-alpine regions.

Models of karst aquifers can provide valuable information about the functioning of the aquifer. Many models were applied to alpine karst aquifers (e.g., Chen & Goldscheider, 2014; Dobler et al., 2013; Hartmann et al., 2012). Distributed karst models discretise the karst system in two- or three-dimensional grids and require the assignment of characteristic hydraulic parameters and system states to each grid cell (Hartmann et al., 2014). Lumped approaches conceptualise the physical processes at the scale of the whole karst system without modelling spatial variability in detail (Hartmann et al., 2014). Such reservoir models usually have a quite simple structure and are well suited to simulate the relation between input (rainfall) and output (discharge at the spring). These models can not only contribute to a better understanding of the aquifer but also provide a valuable tool to manage these aquifers in regard to climate change.

To accurately predict future CO_2 levels in the atmosphere and its consequences for climate change, it is also crucial to quantify the sources and sinks of the greenhouse gas CO_2. Carbonate rock weathering (both dissolution and reprecipitation of carbonate) plays an important role, especially in karst areas (e.g., Hartmann, 2009; Liu & Zhao, 1999).

Within this study, we investigated a high-alpine karst system in Vorarlberg, Austria, which has only one spring as major outlet and very clear catchment boundaries. Such hydrological systems are quite rare but scientifically valuable for water- and mass balance calculations that can then be transferred to other hydrogeological systems with less clear boundaries.

This study aims to provide new insights into the dynamics of high-alpine karst systems using a well-defined catchment as study area. Tracer tests were used to define the catchment of the karst system and confirm that the system acts as sort of a natural lysimeter as it is only drained by one spring. The possible atmospheric CO_2 sink for the studied karst system was calculated according to the hydrochem-discharge method of Liu and Zhao (1999). In addition, the denudation rates for carbonate rocks in the investigated system were calculated and compared to values from other studies and finally, the KarstMod modelling package (Mazzilli et al., 2017) was used to simulate the rainfall-discharge behaviour during time periods not affected by snowmelt. The modelling results were also used to assess the internal flows within the karst aquifer and to demonstrate the importance of the matrix for water storage in low-flow periods.

2 | MATERIALS AND METHODS

2.1 | Study area

The alpine study site Disnergschroef (Figures 1 and 2) is located in the UNESCO Biosphere Reserve Großes Walsertal in the federal state of Vorarlberg in Austria (Figure 2a). The study site receives the highest precipitation amounts in Austria. According to Werner (2007) the mean annual precipitation in the Disnergschroef area is between 2100 mm and about 2700 mm in the peak areas. Depending on the elevation, between 45% and over 60% of the annual precipitation occurs as snow (Werner, 2007). Precipitation data from gauging stations at Koerbersee (1675 m a.s.l.), Sonntag/Stein (1750 m a.s.l.) and Formarinalpe (1880 m a.s.l.), which are located west, east and south-east of the study area, confirm the precipitation variations. Highest precipitation rates are during the summer months, while lowest rates are measured during winter.

The relief of the investigation area (catchment of Gadenalpe spring = QGA, Figures 1d and 2b) ranges from 1400 m a.s.l. to over 2400 m a.s.l. with steep slopes and deep valleys. The Disnergschroef karst area (Figures 1a and 2b) belongs to the Northern Calcareous Alps and consists of a thick Main Dolomite-Limestone complex (Carnian—Norian) with distinct karst features. The karst plateau shows no surface runoff and is characterised by dolines, depressions, shafts and small caves.

The Main Dolomite also constitutes most of the summits surrounding the karst area. The cross section through the investigation area (A'–A, Figure 2c) shows that a main fault separates the Triassic Main

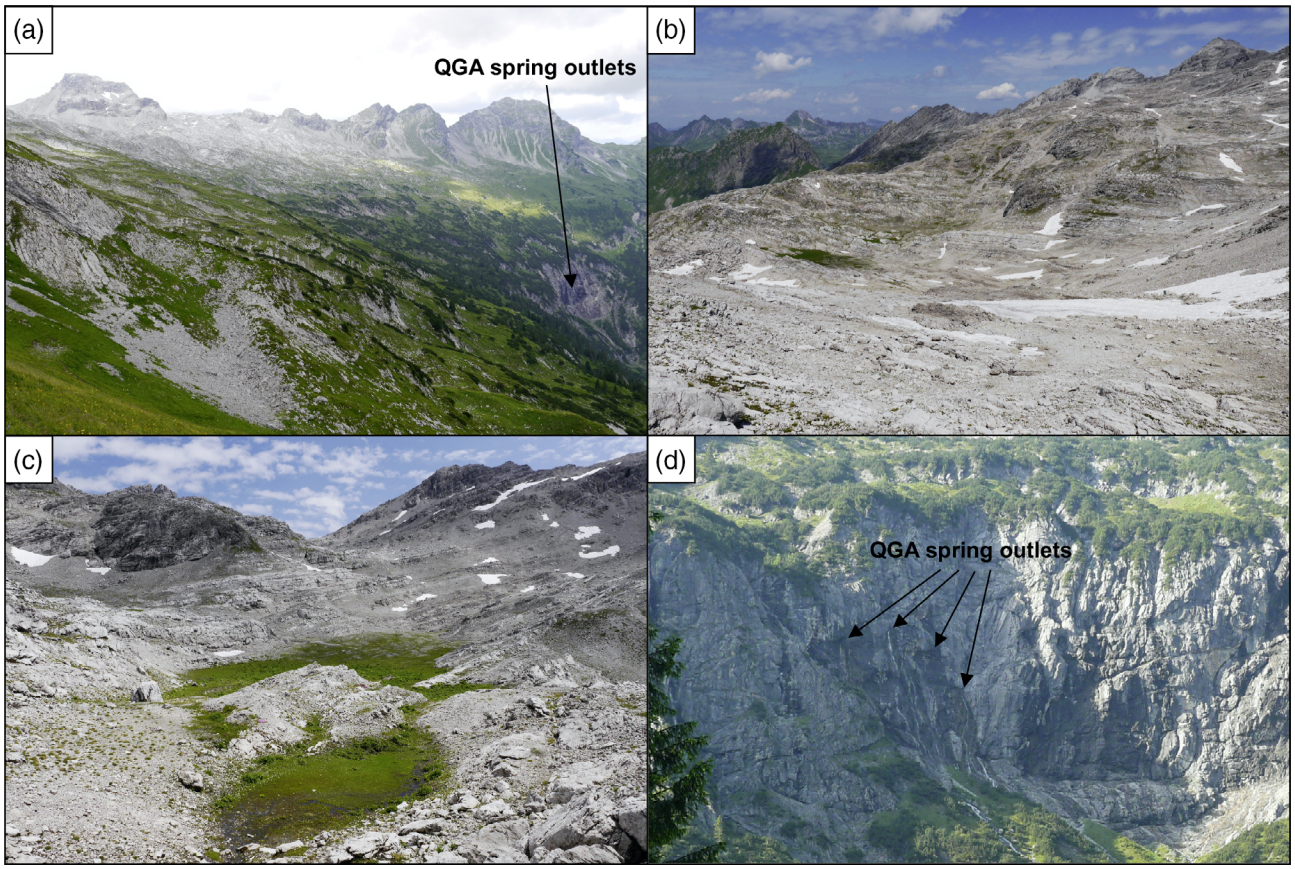

FIGURE 1 (a) Overview of the Disnergschroef karst plateau; (b) top of the karst plateau with typical karst features, dolines and depressions; (c) depression in the karst plateau, where water directly enters the karst aquifer; (d) view of the QGA spring outlets

Dolomite-Limestone formation from Cretaceous and older deposits. The dolomite-limestone formation is underlain by the Raibl Fm. which consists of dark, indurated limestone and slatey, impermeable marls, as well as gypsum and rauhwackes and locally overlain by Jurassic limestone formations. In the area below the spring outlet, the Cretaceous and older deposits are covered by morainic sediments (Figure 2c).

The spring consists of four main outlets very close to each other (Figure 1d, summarised as QGA in the following). The point of measurement (QGA) is a few metres further downstream where the individual spring outlets flow together. The springs emerge from the dolomite/limestone formation.

Above 1800 m a.s.l. most of the area is sparsely covered by alpine vegetation (Figure 1). The study site and the springs are only accessible in the summer month because of high amounts of snow in winter and due to the risk of avalanches.

Two tracer tests (Table 1), performed in July/August 2013 and July/August 2015, indicate that the whole karst plateau is principally drained by QGA. Two kilograms of the fluorescent tracer Amidorhodamine G were used for each tracer test. The injection points were located near the top of the Disnergschroef karst plateau at an elevation of about 2300 m a.s.l. (Figure 2b,c). The tracer was injected into a small stream, fed by snow melt water, which seeps into the karst aquifer a few metres further downstream and had a discharge of about 0.4 L/s.

The injection was conducted after several days without rain.

In total 25 springs and river locations in the Großes Walsertal valley and in the upper Lech valley were investigated with water samples or activated charcoal bags (Figure 2b). Only one sampling location (QGA) led to positive tracer detection results in water samples and charcoal bags. Positive water samples were also collected further downstream following the small stream fed by QGA. All other water samples and charcoal bags were negative. This is evidence that the karst plateau is principally drained by the QGA spring system. The karst plateau can therefore be considered as a sort of natural lysimeter. Such an alpine system is quite unique and scientifically valuable because transferable detailed water and mass balances can be calculated.

2.2 | Hydrological- and physicochemical-data

The QGA spring was monitored continuously from 25.07.2016 to 12.07.2019. Water level (precision ±0.1 cm), water temperature (± 0.1°C) and specific electrical conductivity (EC, ±1 µS/cm) were measured at 15 min intervals with a CTD sensor (Ott Hydromet GmbH, Kempten, Germany). Discharge measurements were undertaken using the salt dilution method with point injection. Water level was converted into continuous discharge using the following stage

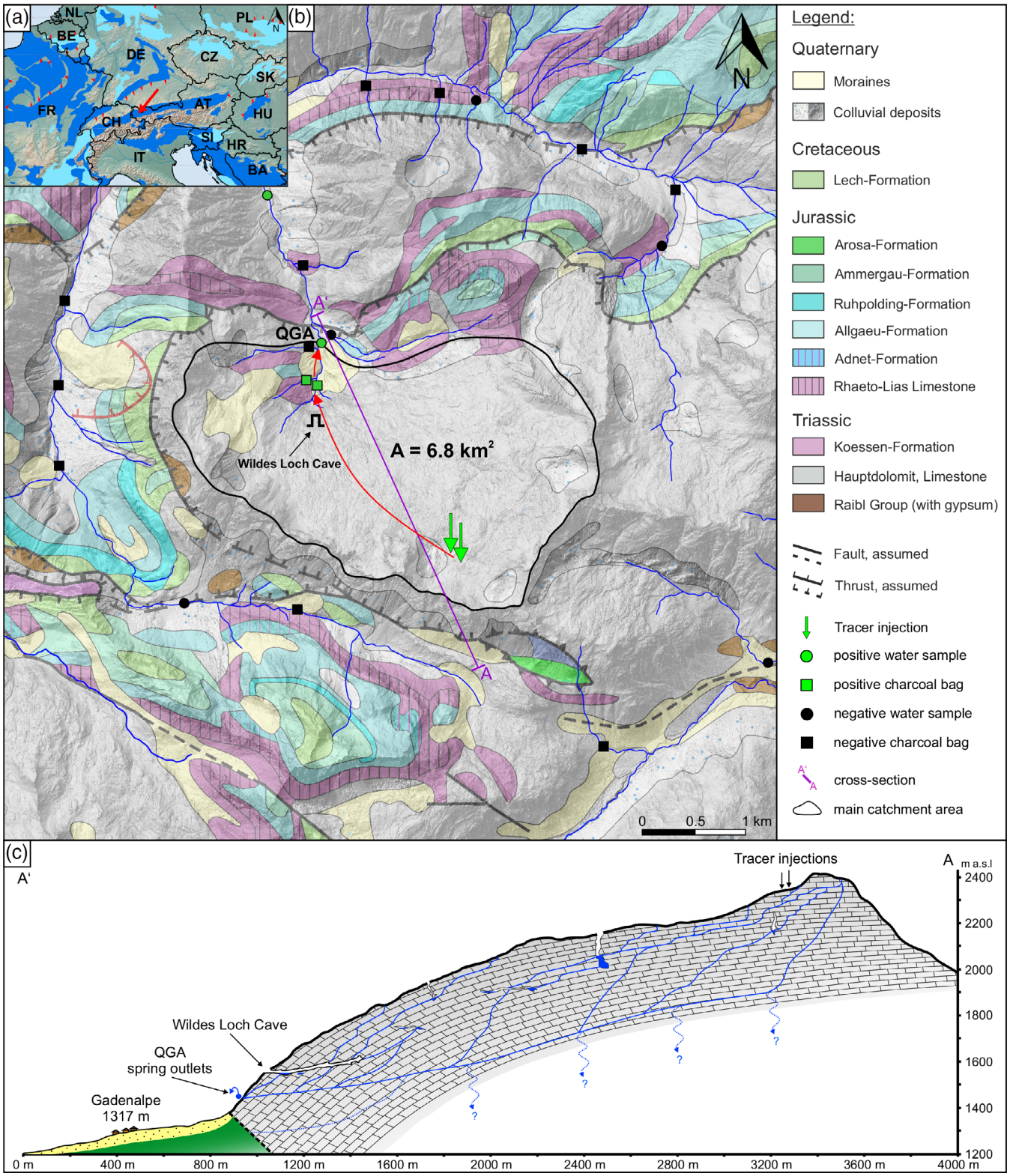

FIGURE 2 (a) Location of the study area in the federal state of Vorarlberg in Austria (basemap: World karst aquifer map, modified after Chen et al., 2017), (b) detailed view of the study site Disnergschroef with the tracer test sampling locations (basemap: Land Vorarlberg—data.vorarlberg.gv.at) and (c) geological cross section through the test site

(x in cm) – discharge (y in L/s) relationship, which was obtained by plotting the 22 measured discharge values versus the corresponding water level data (polynomial regression).

$$y = 1.437x^2 - 8.2128x \quad (1)$$

The obtained R^2 value for the polynomial regression was 0.99.

TABLE 1 Basic parameters and results of the two tracer tests

	Tracer test 2013	Tracer test 2015
Injection quantity	2000 g	2000 g
Spring discharge	335 L/s	275 L/s
Time of first detection	8.5 h	12.1 h
Peak time	13.5 h	17.2 h
Peak concentration	21.5 µg/L	22.1 µg/L
Maximum velocity	229.4 m/h	161.2 m/h
Peak velocity	144.4 m/h	113.4 m/h

Rainfall data were obtained from three stations Koerbersee, Formarinalpe and Sonntag/Stein. For this publication the values of the station Formarinalpe was taken as representative precipitation values.

Potential evapotranspiration (PET in mm/day) was estimated by using the Haude method (DVWK, 1996).

$$\mathrm{PET} = f \cdot (e_{s14} - e_{a14}) \tag{2}$$

$$e_{s14} = 6.11 \cdot 10^{\left(\frac{7.48 \cdot T}{237+T}\right)} \tag{3}$$

$$e_{a14} = U \cdot e_{s14} \tag{4}$$

where f is the Haude factor for the individual months (f = 0.25 for August, f = 0.23 for September, f = 0.22 for October, f = 0.20 for November) and $e_{s14} - e_{a14}$ is the vapour saturation deficit of air (in hPa) at 14:00 MEZ, calculated using measured air temperature (T in °C) and relative humidity U (in %) at 14:00 MEZ. For this calculation, the air temperature and humidity data of the station Koerbersee were taken as humidity data were only available from this station.

To estimate the contribution of carbonate rock weathering to the atmospheric CO_2 sink, the hydrochem-discharge method was employed (Liu & Zhao, 1999). The flux (F) of the atmospheric CO_2 consumed in carbonate rock weathering can be estimated by:

$$F = \frac{1}{2} \cdot \left[\mathrm{HCO_3^-}\right] \cdot Q \cdot \frac{M_{\mathrm{CO_2}}}{M_{\mathrm{HCO_3^-}}} \tag{5}$$

where $[HCO_3^-]$ is the HCO_3^- concentration in water (in g/L), M_{CO_2} and $M_{HCO_3^-}$ are the respective molecular weights (in g/mol), Q is the discharge (in L/s) and ½ means that only half of the carbon in solution is from atmospheric CO_2 (Liu & Zhao, 1999).

Alkalinity was measured as triplicate by volumetric titration on site, using an alkalinity test (Merck KGaA, Darmstadt, Germany) and the mean value was taken as result. In total, 34 alkalinity measurements were conducted in different time intervals and during different hydrological conditions. The 34 individual bicarbonate concentrations were plotted versus the EC measured at the same time. A continuous bicarbonate time series was then obtained by a linear regression (Figure 3).

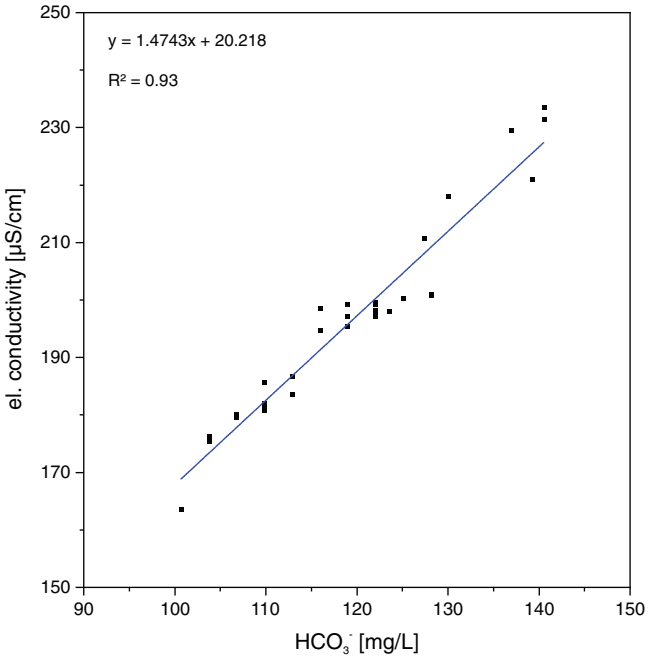

FIGURE 3 Relation between bicarbonate and electrical conductivity

2.3 | Modelling with KarstMod

The modelling platform KarstMod (Mazzilli et al., 2017) is dedicated to karstic groundwater flow simulation. It provides an adjustable modelling platform for discharge simulations and hydrodynamic analysis and can reproduce the conceptual structure of karst models known in the literature (e.g., Butscher & Huggenberger, 2008; Fleury et al., 2007). The model is set up as a two-level structure. Level 1 consists of compartment E (soil and epikarst), which represents the infiltration zone and is influenced by precipitation (P) and evapotranspiration (ET). The water flows then to the second level, which consists of compartments C (conduits), M (matrix) and L (highly capacitive matrix) which represent the different sub-systems of the saturated zone (Sivelle et al., 2019). The configuration of the KarstMod reservoir model used in this study is shown in Figure 4. For better realism, all output discharge is set through reservoir C and compartment L is not used as the investigated system is a very responsive watershed.

The modelling is based on the balance equations given by Mazzilli et al. (2017) and consists of compartments E, M and C.

$$\frac{dE}{dt} = P - \mathrm{ET} - Q_{\mathrm{EM}} - Q_{\mathrm{EC}} \tag{6}$$

$$\frac{dM}{dt} = Q_{\mathrm{EM}} - Q_{\mathrm{MC}} \tag{7}$$

$$\frac{dC}{dt} = Q_{\mathrm{EC}} + Q_{\mathrm{MC}} \tag{8}$$

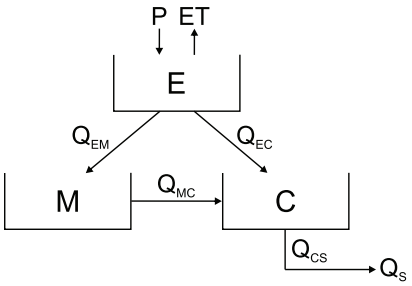

E: Reservoir E (epikarst)
M: Reservoir M (matrix)
C: Reservoir C (conduit)
P: Precipitation
ET: Evapotranspiration
Q_S: Spring Discharge
Q_{EM}, Q_{EC}, Q_{MC}, Q_{CS}: water flow between compartments

FIGURE 4 Structure of the selected rainfall-discharge reservoir model

$$Q_{EM} = k_{EM} \times E_t \text{ if } E_t > 0, \text{otherwise } Q_{EM} = 0 \quad (9)$$

$$Q_{EC} = k_{EC} \times (E_t - E_{ThresholdC}) \text{ if } E_t > E_{ThresholdC}, \text{otherwise } Q_{EC} = 0 \quad (10)$$

$$Q_{MC} = k_{MC} \times [M(t) - C(t)] \quad (11)$$

$$Q_{CS} = k_{CS} \times C_t \quad (12)$$

E_t, M_t and C_t are the water levels in the epikarst, matrix and conduit reservoirs. k_{AB} is the recession coefficient associated with the flow from reservoir E → M, E → C, M → C and C → S. Q_{AB} is the discharge from A to B (e.g., E → C) and is computed by the product of Q_{AB} (e.g., Q_{EC}) and the total surface of the recharge area (R_A). With the model configuration chosen for this study, the discharge at the outlet Q_S is given by:

$$Q_S = R_A \times Q_{CS} \quad (13)$$

The rainfall-discharge model is calibrated using a quasi-Monte-Carlo procedure with a Sobol sequence sampling of the parameter space (Mazzilli et al., 2017; Sobol, 1977). The performance criteria in KarstMod are the Nash-Sutcliffe efficiency coefficient (NSE, Nash & Sutcliffe, 1970) and the modified balance error (BE), defined as follows:

$$NSE = 1 - \frac{\sum (Q_{obs} - Q_{sim})^2}{\sum (Q_{obs} - Q_{mean})^2} \quad (14)$$

$$BE = 1 - \left| \frac{\sum (Q_{obs} - Q_{sim})}{\sum Q_{obs}} \right| \quad (15)$$

where Q_{obs} is the observed discharge, Q_{sim} is the simulated discharge and Q_{mean} is the average observed discharge. An NSE of one is a perfect match between model and observations while an NSE of 0 indicates that the model performs equally to the mean of the observed data. A BE of one means that the simulated discharge is equal to the observed discharge. The KarstMod platform uses an aggregated objective function defined as the weighted sum of the two performance criteria (Baudement et al., 2017) according to equation:

$$W_{obj} = w\text{NSE} + (1 - w)\text{BE} \quad (16)$$

With W_{obj} as the objective function and w as the weight defined by the user ($0 \le w \le 1$). In this study we used $w = 0.9$. KarstMod proposes to use the simulation results from all parameter sets with a $W_{obj} > 0.7$ to evaluate the uncertainty of the simulation results. This approach is derived from the Regional Sensitivity Analysis (Hornberger & Spear, 1981) and the Generalised Likelihood Uncertainty Estimation (Beven & Binley, 1992).

In the model, three periods must be taken into account, the warm-up, calibration and validation periods. The warm-up period corresponds to the time interval after which the initialisation bias is deemed to be negligible (Baudement et al., 2017). The simulation results of this period are not considered for the calibration.

For this study, time periods during summer and autumn (August–November 2016 and 2017, August–October 2018), which are not influenced by snowmelt, were chosen for three consecutive years (2016–2018) for modelling in order to simulate the rainfall-discharge behaviour and the internal flows within the karst aquifer as a reaction to rainfall events.

A sensitivity analysis was also carried out, using all parameter sets with $W_{obj} \ge 0.7$. Indices are calculated using the Sobol procedure as described in Saltelli (2002). The sensitivity index S_i for parameter X_i with respect to the simulated discharge Q_S is defined as the fraction V_i of the variance V (Q_S) of the simulated discharge, which is due solely to the parameter X_i (Baudement et al., 2017).

$$S_i = \frac{V_i}{V_{Q_S}} \quad (17)$$

The total sensitivity index S_{Ti} measures the contribution of X_i to the output variance, including the interactions of X_i, of any order, with other input variables (Saltelli et al., 2008). By default, the sensitivity indices provided by KarstMod are obtained based on $N = 1000 \times (n_{par} + 2)$ parameter set, where n_{par} is the number of parameters to be calibrated (Baudement et al., 2017).

3 | RESULTS AND DISCUSSION

3.1 | Temporal evolution of discharge, EC and bicarbonate

During the investigation period from 25. July 2016 to 12. July 2019, the cumulative rainfall was 6287 mm (Table 2). The temporal

TABLE 2 Table 1: Overview of the values for mean discharge, mean EC, mean bicarbonate, mean bicarbonate flux and rainfall for different time periods

Time	Mean discharge (L/s)	Mean EC (µS/cm)	Mean HCO_3^- (mg/L)	Mean HCO_3^--flux (g/s)	Sum rainfall (mm)
Total period	237	168	100	22.5	6284
Hydrological year (Nov. 16–Oct. 17)	335	166	99	38.0	2218
Hydrological year (Nov. 17–Oct. 18)	164	159	94	14.0	1759
Low-flow (Nov. 16–Feb. 17)	137	194	118	24.4	403
Low-flow (Nov. 17–Feb. 18)	197	160	95	18.4	839
Low-flow (Nov. 18–Feb. 19)	20	186	113	2.2	749
Snowmelt (March 17–June 17)	371	158	94	33.9	706
Snowmelt (March 18–June 18)	205	145	85	14.9	389
Snowmelt (March 19–June 19)	254	179	108	18.4	623

evolution of the monitored parameters discharge, EC and rainfall are shown as time series in Figure 5. The hydrograph reveals distinct increases in response to recharge events with a delay of only a few hours, as also observed by many other studies of karst aquifers (e.g., Frank et al., 2019; Mudarra & Andreo, 2010; Vigna & Banzato, 2015). The highest discharge values, with up to 2200 L/s, were recorded after major rainfall events in the summer month of 2016, 2017 and 2019. Low-flow values during time periods without rainfall in autumn and winter are as low as 10 L/s. The mean discharge for the whole investigation period was 237 L/s. After each recharge period, EC rose progressively during the recession period until the next rainfall event. The mean EC for the whole period was 168 µS/cm.

The bicarbonate flux of the investigated spring was obtained using the calculated continuous HCO_3^- data and the according discharge values. The flux varies between 1 g/s and over 210 g/s after heavy rain events with a mean of 22.5 g/s. The exceptionally dry summer 2018 shows clearly the lowest discharge values and accordingly the lowest bicarbonate flux. Table 2 gives an overview of the previously mentioned parameters for different time periods.

The mean discharge is significantly lower for the hydrological year 2017/2018 compared to the hydrological year 2016/2017 because of the dry summer 2018. Accordingly, the rainfall during the hydrological year 2016/2017 was almost 500 mm more compared to 2017/2018. The mean discharge during the snowmelt periods is always greater compared to low-flow periods in autumn and winter (Table 2). The mean EC is greater during low-flow periods and accordingly the calculated mean bicarbonate concentration is greater during low-flow. Because discharge is always higher during snowmelt, the calculated mean bicarbonate flux is therefore more or less the same. An exception is the low-flow period from November 2018 to February 2019 because of the exceptionally dry summer 2018. The rainfall during the period March 2018 to June 2018 was only 389 mm while during the same periods in the year 2017 and 2019, the rainfall is two times higher. During this period in 2018, the mean discharge is as low as 20 L/s and accordingly the mean bicarbonate flux is also very low.

For the time periods August–November 2016, August–November 2017 and August–October 2018 (used for modelling and not influenced by snow melt), cross-correlations were calculated to compare rainfall with the discharge and EC behaviour of the investigated spring (Figure 6). Highest correlation was found for rainfall versus discharge with a time lag of 5.5 h. Negative correlations were calculated for rainfall versus EC and for discharge versus EC. The time lag for rainfall versus EC is 8.5 h while the time shift for discharge versus EC is 3.0 h. This means that discharge starts to rise 5.5 h after the rain event and EC starts to decrease about 8 h after the rain event. The time lag between increase of discharge and decrease of EC likely results from a hydraulic pressure pulse, also known as piston effect (Ravbar et al., 2011). These results also coincide with the results obtained from the tracer tests, where time of first detection was 8.5 h after the injection.

3.2 | Denudation rates and carbonate rock weathering

By using hydrochemical and discharge data, the flux of atmospheric CO_2 consumed in carbonate rock weathering can be estimated using Formula (5). The CO_2 sink was calculated for different time periods, given in Table 3. During the three investigated low-flow periods (November 2016–February 2017, November 2017–February 2018, November 2018–February 2019) the CO_2 sink varies between 3.7 and 31.3 t/a/km^2. The very low value of 3.7 t/a/km^2 is again related to the very dry summer 2018. Accordingly, the estimated transient CO_2 sink for the investigated karst plateau is between 25.2 and 212.8 t/a during low-flow. For the snowmelt periods (March 2017–June 2017, March 2018–June 2018 and March 2019–June 2019) the

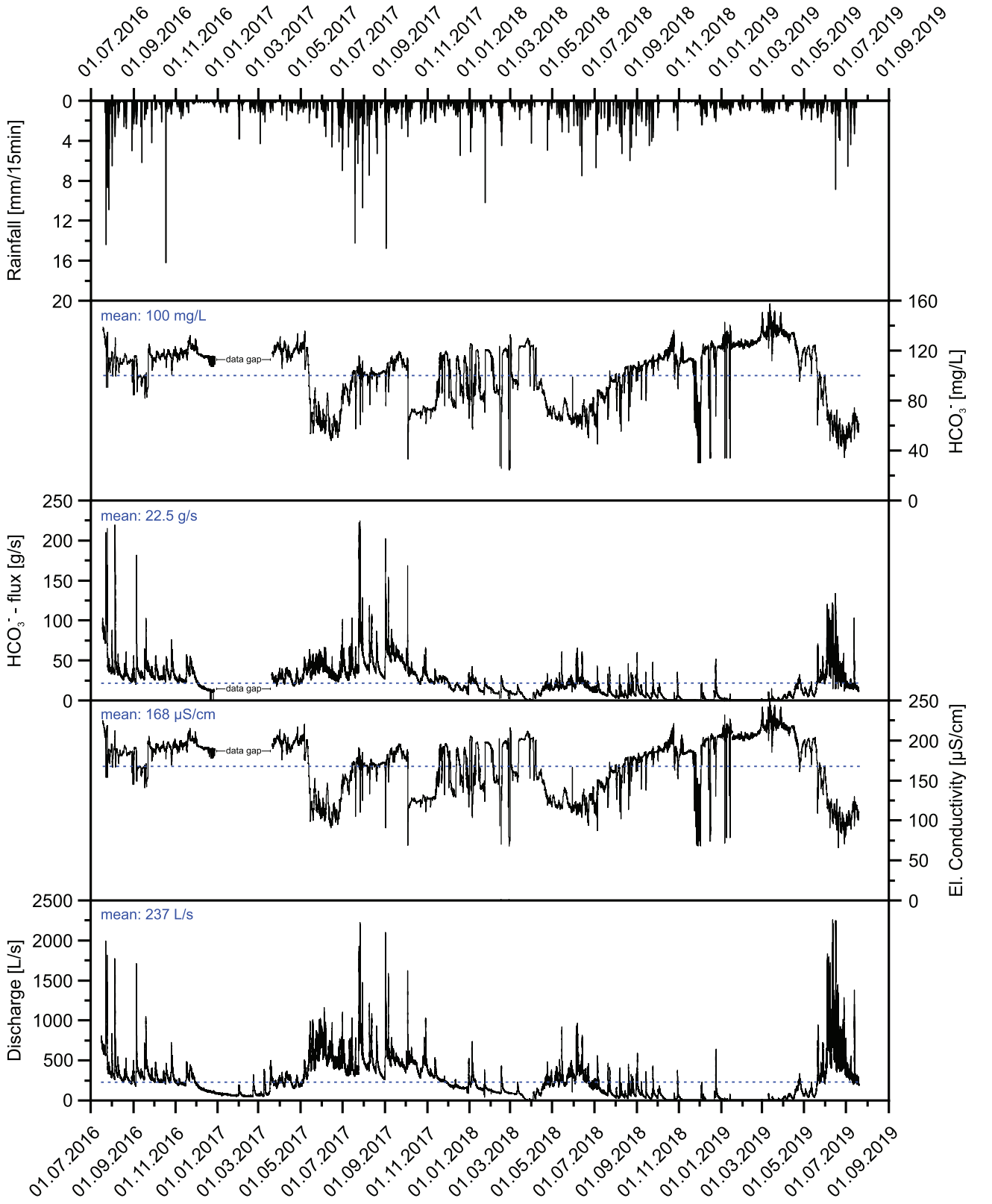

FIGURE 5 Time series of rainfall, electrical conductivity and discharge of the investigated spring as well as calculated bicarbonate concentration and bicarbonate flux

CO_2 sink varies between 29.1 and 58.3 t/a/km^2. Again, the lowest value is related to the dry summer 2018. For the whole karst plateau, the transient CO_2 sink is between 197.9 and 396.4 t/a. during snowmelt. For the whole investigation period, the calculated atmospheric CO_2 sink is 39.7 t/a/km^2 which means 270 t/a for the entire karst plateau.

Table 3 gives an overview of the relevant parameters for the calculation of the CO_2 sink.

These values show that the investigated karst system contributes to the atmospheric CO_2 sink, at least on relatively short time scales. These results can also contribute to a better understanding and prediction of future CO_2 levels in the atmosphere.

Other studies of the atmospheric CO_2 sink in alpine regions also found that the CO_2 sink is about four times higher in the melting season compared to the freezing season, because the effect of higher flow rates overrides the effect of lower bicarbonate concentrations (Zeng et al., 2012). Our study also shows higher values during the melting season but approximately only two times higher compared to low-flow periods. Other studies also showed that CO_2 consumption by chemical weathering is highly sensitive to climate change, especially to changes in precipitation, temperature and runoff patterns (Hartmann, 2009), which is especially important for the alpine region and can be seen during the dry summer period in 2018 in this study.

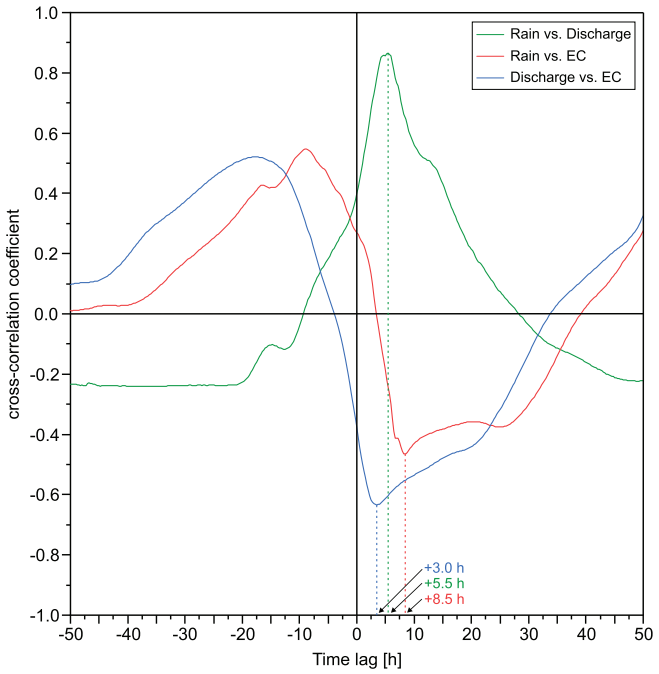

FIGURE 6 Cross correlation between time series of rainfall, discharge and electrical conductivity (for the same periods that were used for modelling). There is a slight time lag of a few hours between each correlation

In addition to the CO_2 sink, the denudation rates for calcite and dolomite in the investigated system were also calculated, assuming that pure calcite and pure dolomite occur as a mixture in the aquifer. The denudation rate is considered as the rate of lowering of a karst surface due to the chemical dissolution of bedrocks (Gabrovsek, 2009). Kaufmann & Braun (2001) showed that denudation processes result in a landscape evolution almost twice as effective as the purely erosional evolution of an insoluble landscape. Denudation rates depend on climatic, lithological and structural factors (Gabrovsek, 2009). Input parameters are the mean Ca^{2+} concentration (15 individual measurements) with 21.1 mg/L and the mean Mg^{2+} concentration (15 individual measurements) with 9.9 mg/L. The denudation rates were calculated for the hydrological year 2016/2017 and for the hydrological year 2017/2018. The assumed runoff was 335 L/s (2016/2017) and 164 L/s (2017/2018) respectively and the recharge area is 6.8 km^2. The density of pure calcite is 2.7 t/m^3 and 2.9 t/m^3 for pure dolomite.

Approximately 126 t/a of calcite are removed from the system by dissolution, which equals a calcite denudation rate of 6.9 mm/1000 years. Some 794 t/a of dolomite are removed from the system annually, which means a denudation rate of 40.2 mm/1000 years. In total, the calculated denudation rate for the carbonate rocks in the investigated system is therefore 47.1 mm/1000 years, calculated with values of the hydrological year 2016/2017. With values of the following hydrological year, 62 t/a of calcite and 389 t/a of dolomite are removed from the system, which equals a denudation rate of 3.4 mm/1000 years for calcite and 19.7 mm/1000 years for dolomite. In total, the denudation rate for carbonate rocks is 23.1 mm/1000 years.

TABLE 3 Time periods and relevant parameters for the calculation of the CO_2 sink

Test site	Time period	Area (km^2)	HCO_3^- concentration (g/L)	Runoff module (L/s/km^2)	Atmospheric CO_2 sink [t/a/km^2]
Disnergschroef (A)	Total period	6.8	0.100	34.9	39.7
	Hyd. Year (Nov. 16–Oct. 17)	6.8	0.099	49.3	55.5
	Hyd. Year (Nov. 17–Oct. 18)	6.8	0.094	24.1	25.8
	Nov. 16–Feb. 17	6.8	0.118	20.1	27.0
	Nov. 17–Feb. 18	6.8	0.095	29.0	31.3
	Nov. 18–Feb. 19	6.8	0.113	2.9	3.7
	March 17–June 17	6.8	0.094	54.6	58.3
	March 18–June 18	6.8	0.085	30.1	29.1
	March 19–June 19	6.8	0.108	37.4	45.9

The main factors affecting denudation rates are climate (infiltration, temperature and the amount of CO_2 available) and lithology (Appelo & Postma, 2005; Dreybrodt, 1988; Gabrovsek, 2009). The denudation rates, calculated in other studies, vary between 4 and 193 mm/1000 years (Figure 7).

The relation between the denudation rate of carbonate rocks and runoff (Figure 7) clearly reflects the sensitivity of denudation and carbonate rock weathering from the runoff change. The larger the runoff, the more intensive is the carbonate rock weathering and denudation. The calculated values from the investigated system are about 40%–60% lower compared to expected values (Figure 7). The reason for that might be either the quite low mean annual temperature in this area or the general geological situation. The rocks in the study area are described as dolomite/limestone formation while the majority is less soluble dolomite.

3.3 | Modelling results with KarstMod

The model has been calibrated and validated for the outlet of the karst plateau (QGA) using hourly data for discharge and rainfall. The observed and modelled discharge together with the rainfall during the investigation period are given in Figure 8a,c. Time periods not influenced by snowmelt were chosen (August–November 2016 and 2017, August–October 2018), in order to reduce the uncertainty of the model introduced by snowmelt and to simulate the direct reaction to rainfall events.

According to the performance criteria (Table 4) and the shape of the simulated discharge curves, the model shows a good fit to the observed data. The NSE is 0.83 for the calibration period and 0.76 for the validation for the simulated time period in 2016. The BE is close to one for both, the calibration period and the validation period. The objective function gives values of 0.85 for the calibration period and 0.76 for the validation period. The objective function for the time periods 2017 and 2018 shows values of 0.79 and 0.72 for the calibration period and values of 0.72 and 0.74 for the validation period respectively. All performance criteria parameters are given in Table 4. These performance values are similar to those from other studies using KarstMod (e.g., Baudement et al., 2017; Poulain et al., 2018; Sivelle et al., 2019).

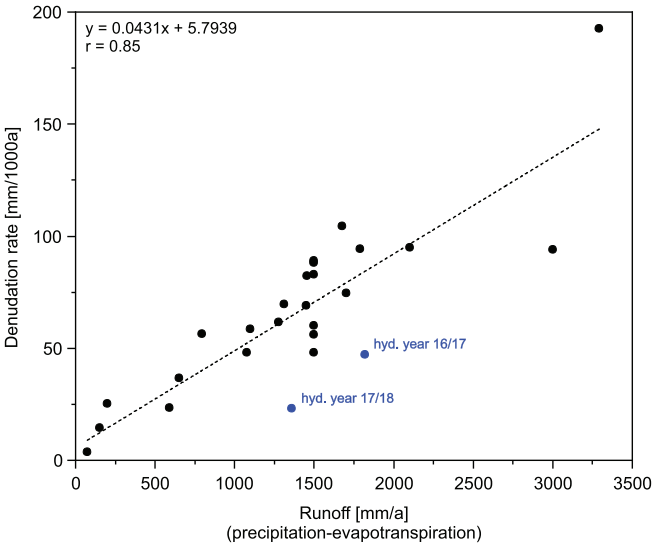

FIGURE 7 Relation between denudation rate of carbonate rocks and runoff. Data from Bakalowicz (1979), Gams (2004), Gunn (1981), Kunaver (1979), Plan (2005), Yoshimura and Inukura (1997), White (1984)

The optimum value determined for the recharge area is 6.9 km^2. This modelling result confirms the delineation of the recharge area by geographical and geological information (6.8 km^2, see Figure 2b) and also demonstrates that the karst system is mainly drained by the investigated QGA spring.

All simulations (10,000) with a performance criteria $W_{obj} > 0.7$ for the simulated period in 2016 are, as an example, graphically represented in Figure 9. For each parameter calibrated, a scatterplot of the values of the objective function (calibration period) against the values of the parameter is given. Based on a equifinality analysis, these plots show that the model has found an optimum for the calibration. The parameter set associated with the highest performance criteria was kept and used to draw the simulated discharge curve given in Figure 8.

As an example, the first-order and total-effect sensitivity indices for the simulated period in 2016 are given in Table 5. The total-effect index indicates the overall sensitivity of the model performance (assessed by the objective function) to the parameters, within the previously user-defined range of variations. The most sensitive parameters are k_{MC}, R_A and k_{EC}, while the least sensitive parameters are k_{EM} and k_{CS}.

Considering the internal flow dynamics of a karst aquifer is important to quantify potential pollution but also to predict and manage spring discharge scenarios regarding climate change. Figure 8b gives an overview of the internal flows between the different compartments of the KarstMod model.

The flow from compartment *E* (epikarst) to compartment *C* (conduit) is highly variable, depending on the input signal (rainfall). Considering future climate scenarios (with more heavy rainfall events) this highly variable flow might become even more variable. The highest internal flow with the highest variability (also depending on the input signal) occurs between *E* and *M* (matrix). Again, taking more heavy rainfall events into account, the variability of this flow might also increase, but the matrix itself will act as a buffer up to a certain limit. Internal flow from *M* to *C* is more or less constant for the three investigation periods with only slight increases directly after rainfall events, when the whole water level in the system rises. The matrix acts as a buffer and a storage for water and slowly releases the water into the conduits and thence to the spring (Figure 8b). Matrix storage is therefore particularly important for the discharge of the spring during low-flow periods (baseflow).

This modelling result also matches the geological setting in the investigated system. The Main Dolomite-Limestone formation is several hundred metres thick and can act as a large (matrix) storage for

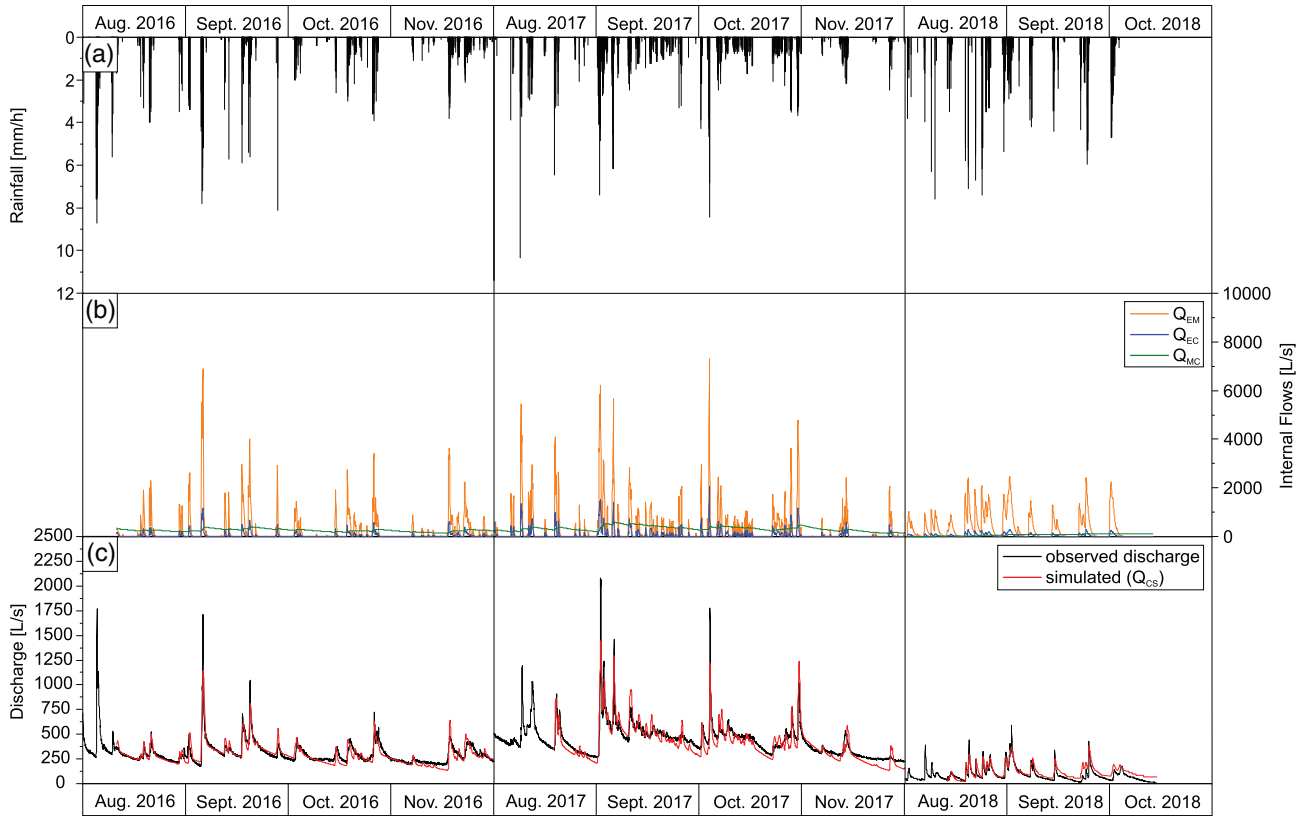

FIGURE 8 (a) Rainfall during the investigation periods in 2016, 2017, and 2018, together with (b) the internal flows between the different compartments and (c) observed and simulated discharge values for the time periods in 2016, 2017, and 2018

TABLE 4 Performance of the model for calibration and validation period of each simulation period

Performance criteria	Calibration period			Validation period		
Time period	**2016**	**2017**	**2018**	**2016**	**2017**	**2018**
NSE	0.83	0.78	0.69	0.76	0.70	0.74
BE	0.99	0.95	0.99	0.99	0.92	0.74
W_{obj} = 0.9 NSE + 0.1 BE	0.85	0.79	0.72	0.76	0.72	0.74

Abbreviations: BE, balance error; NSE, Nash Sutcliff efficiency; W_{obj}, objective function.

water. The importance of the matrix storage for the whole karst aquifer becomes evident, considering that the spring almost never falls dry, even during long dry periods and is therefore mainly responsible for the baseflow of the spring.

A conceptual model of the internal flow dynamics inside the investigated system is given in Figure 10.

Other models of karst aquifers (e.g., Baudement et al., 2017; Chen & Goldscheider, 2014; Loncar et al., 2018) also show that the resulting hydrographs are composed of rapid-flow and slow-flow components (baseflow, M → C) as described by, for example, Ford and Williams (2007). Our modelling results clearly show the importance of the matrix storage, which is also an important factor for future management strategies, considering that climate change scenarios project more heavy rainfall events, but also longer dry periods. The model is also able to reproduce the reaction of the spring to rainfall events, which again is important, taking into account more heavy rainfall events in the future.

4 | CONCLUSION

With these investigations in a high-alpine karst system with a clearly defined catchment, we obtained new and improved knowledge about the dynamic water and mass balances of alpine karst systems.

Tracer tests show that the investigated karst plateau has only one major spring as outlet. The surface catchment area of this spring is about 6.8 km^2 which was also confirmed by the KarstMod model (6.9 km^2).

While the observed discharge values show a rapid and marked increase after rainfall events, the recorded specific EC values decrease

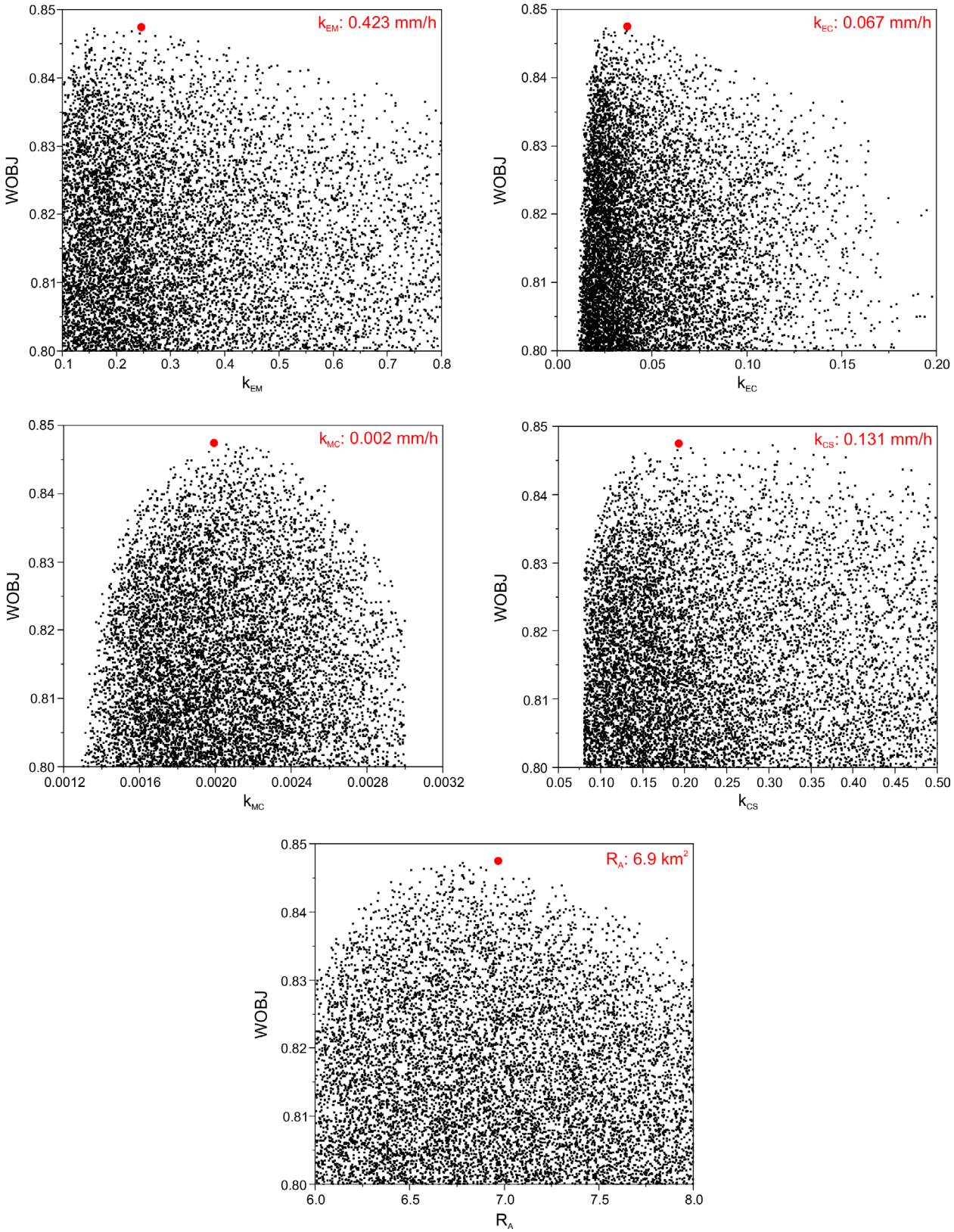

FIGURE 9 Analysis of the sensitivity of the input parameters of the rainfall-discharge model (2016) with a Monte-Carlo procedure. W_{obj} = objective function. The best fit with the objective function chosen is marked with a red dot and the respective value is given for each parameter

accordingly. Measured and calculated bicarbonate values react the same way to rainfall events as EC. The bicarbonate-EC relation illustrates that bicarbonate is the major anion as the karst system consists of a mixture of limestone and dolomite. The calculated bicarbonate flux at the investigated spring QGA varies between 1 and over 210 g/s.

The calculated value for the atmospheric CO_2 sink for the Disnergschroef area is 39.7 t/a/km^2 (mean value for the whole investigation period). This value is lower compared to areas with pure limestone outcrops for example, in southern and northern China. However, there is still a significant contribution of carbonate rock weathering to the transient atmospheric CO_2 sink in the study area. Results of this study also show that the melting period contributes more to the CO_2 sink then low-flow conditions, because the higher discharge overrides the lower bicarbonate concentrations as also shown by Zeng et al. (2012). Nevertheless, future research is needed to evaluate the effect of the CO_2 sink in longer time scales (e.g., CO_2 degassing again from the river back to the atmosphere) or if this effect permanently removes CO_2 from the atmosphere.

The calculated denudation rate for carbonate rocks in our study site is between 23.1 mm/1000 years and 47.1 mm/1000 years, which is slightly lower compared to other studies of karst areas in Europe (e.g., Plan, 2005). The reason for this might be different climatic and geological conditions.

TABLE 5 Sensitivity indices (first-order index and total-effect index) for the simulated time period in 2016

Parameter	First-order index (S_i)	Total-effect index (S_{Ti})
k_{MC}	0.58	0.66
R_A	0.08	0.16
k_{EC}	0.11	0.15
k_{EM}	0.08	0.10
k_{CS}	0.07	0.07

Within this study, a reservoir model, based on KarstMod, has been applied to the Disnergschroef karst system. Based on this model, the internal flow dynamics of the karst system and the reaction of the system to rainfall events could be described. The simulated discharge curves show a good fit to the measured discharge curves. Furthermore, the performance criteria of the model compared to the measured discharge values show that KarstMod is a valuable tool to simulate the discharge behaviour of the investigated spring in response to rainfall events. The model also gives information about the internal flows between the different model compartments. The highest variability of the internal flow was observed between epikarst and matrix, while the flow from matrix to conduits is almost constant and is responsible for the observed baseflow at the spring. This demonstrates the importance of the matrix as water storage especially during dry conditions, which is an important factor as climate change scenarios project more heavy rainfall events but also more and longer dry periods in the future, especially in alpine regions. On the other hand, the matrix can act as sort of a buffer after heavy rain events. As the model is also able to reproduce the reaction of the spring to heavy rainfall events, it could be used as a management tool to forecast flood events, which are predicted to occur more often in the future.

Future KarstMod model applications in alpine regions should consider snowmelt periods and should couple runoff models with mass transport models, for example, to simulate the CO_2 sink of karst areas. These kind of models and the information obtained can be of major interest for the management of karst springs, especially in regard to flood events occurring after heavy rainfall events, and also to assess the effects of climate change in alpine areas.

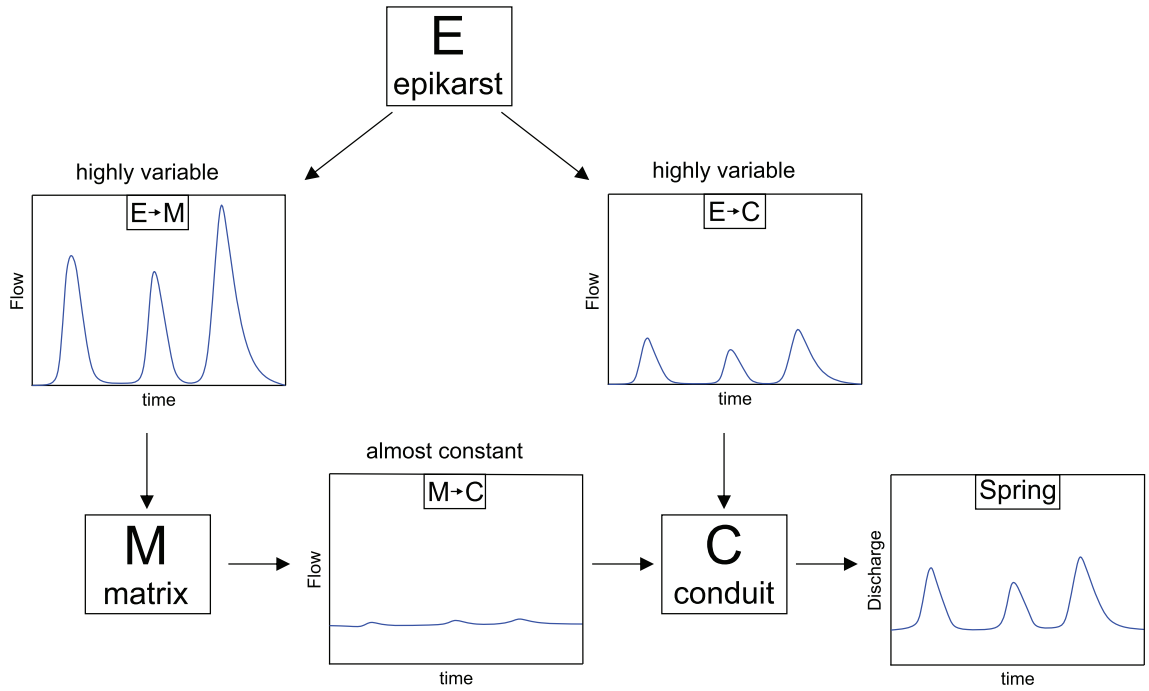

FIGURE 10 Conceptual model of the flow dynamics inside the investigated karst aquifer. E → C = flow from compartment E to C, E → M = flow from compartment E to M and M → C = flow from compartment M to C and spring discharge

ACKNOWLEDGEMENTS

The study was partly funded by the European Commission through the FP7 Marie Curie CIG grant IMKA [grant agreement number 303837]. Financial support of the Federal Ministry of Education and Research (BMBF) and the European Commission through the Partnership for Research and Innovation in the Mediterranean Area (PRIMA) programme under Horizon 2020 (KARMA project, grant agreement number 01DH19022A) is gratefully acknowledged. The authors thank the Water Management Department of the Vorarlberg State Administration for providing rainfall data. Special thanks are given to Kerstin Faust for her valuable help during field work and to David Drew (Dublin, Ireland) for proofreading the original manuscript. Open Access funding enabled and organized by Projekt DEAL.

DATA AVAILABILITY STATEMENT

The data that support the findings of this study are available from the corresponding author upon reasonable request.

ORCID

Simon Frank https://orcid.org/0000-0001-6290-2243

REFERENCES

Appelo, C. A. J., & Postma, D. (2005). *Geochemistry, groundwater and pollution* (p. 649). A.A. Balkema.

Bakalowicz, M. (1979). *Contribution de la géochimie des eaux à la connaissance de l'aquifère karstique et de la karstification* (p. 269). Univ. P. et M. Curie, Paris V, Paris.

Bakalowicz, M. (2005). Karst groundwater: A challenge for new resources. *Hydrogeology Journal*, *13*, 148–160.

Baudement, C., Arfib, B., Mazzilli, N., Jouves, J., Lamarque, T., & Guglielmi, Y. (2017). Groundwater management of a highly dynamic karst by assessing baseflow and quickflow with a rainfall-discharge model (Dardennes springs, SE France). *Bulletin de la Société Géologique de France*, *188*, 40.

Beven, K., & Binley, A. (1992). The future of distributed models: Model calibration and uncertainty prediction. *Hydrological Processes*, *6*, 279–298.

Birk, S., Liedl, R., & Sauter, M. (2004). Identification of localised recharge and conduit flow by combined analysis of hydraulic and physico-chemical spring responses (Urenbrunnen, SW-Germany). *Journal of Hydrology*, *286*, 179–193.

Butscher, C., & Huggenberger, P. (2008). Intrinsic vulnerability assessment in karst areas: A numerical modelling approach. *Water Resources Research*, *44*, 3.

Chen, Z., Auler, A. S., Bakalowicz, M., Drew, D., Griger, F., Hartmann, J., … Goldscheider, N. (2017). The world karst aquifer mapping project: Concept, mapping procedure and map of Europe. *Hydrogeology Journal*, *25*, 1–15.

Chen, Z., & Goldscheider, N. (2014). Modelling spatially and temporally varied hydraulic behavior of a folded karst system with dominant conduit drainage at catchment scale, Hochifen-Gottesacker, Alps. *Journal of Hydrology*, *514*, 41–52.

Dobler, C., Bürger, G., & Stötter, J. (2013). Simulating future precipitation extremes in a complex alpine catchment. *Natural Hazards and Earth System Sciences*, *13*, 263–277.

Dreybrodt, W. (1988). *Processes in karst systems: Physics, chemistry and geology* (p. 288). Springer-Verlag.

DVWK. (1996). *Ermittlung der Verdunstung von Land- und Wasserflächen*. Wirtschafts- und Verl.-Ges., Gas und Wasser.

Filippini, M., Squarzoni, G., De Waele, J., Fiorucci, A., Vigna, B., Grillo, B., … Gargini, A. (2018). Differentiated spring behavior under changing hydrological conditions in an alpine karst aquifer. *Journal of Hydrology*, *556*, 572–584.

Fleury, P., Plagnes, V., & Bakalowicz, M. (2007). Modelling of the functioning of karst aquifers with a reservoir model: Application to Fontaine de Vaucluse (south of France). *Journal of Hydrology*, *345*, 38–49.

Ford, D., & Williams, P. (2007). *Karst hydrogeology and geomorphology*. Wiley.

Frank, S., Goeppert, N., Ohmer, M., & Goldscheider, N. (2019). Sulfate variations as a natural tracer for conduit-matrix interaction in a complex karst aquifer. *Hydrological Processes*, *33*, 1292–1303.

Gabrovsek, F. (2009). On concepts and methods for the estimation of dissolution denudation rates in karst areas. *Geomorphology*, *106*, 9–14.

Gams, I. (2004). *Kras v Sloveniji v prostoru in casu* (p. 515). ZRC Publishing.

Goldscheider, N. (2005). Fold structure and underground drainage pattern in the alpine karst system Hochifen-Gottesacker. *Eclogae Geologicae Helvetiae*, *98*, 1–17.

Goldscheider, N., Chen, Z., Broda, S., Auler, A. S., Bakalowicz, M., Drew, D., … Veni, G. (2020). Global distribution of carbonate rocks and karst water resources. *Hydrogeology Journal*, *28*, 1661–1677.

Gunn, J. (1981). Limestone solution rates and processes in the Waitomo district, New Zealand. *Earth Surface Processes and Landforms*, *6*, 427–445.

Hartmann, A., Goldscheider, N., Wagener, T., Lange, J., & Weiler, M. (2014). Karst water resources in a chnaging world: Review of hydrological modeling approaches. *Reviews of Geophysics*, *52*, 218–242.

Hartmann, A., Kralik, M., Humer, F., Lange, J., & Weiler, M. (2012). Identification of a karst system's intrinsic hydrodynamic parameters: Upscaling from single springs to the whole aquifer. *Environmental Earth Sciences*, *65*, 2377–2389.

Hartmann, J. (2009). Bicarbonate-fluxes and CO_2-consumption by chemical weathering on the Japanese archipelago–Application of a multi-lithological model framework. *Chemical Geology*, *265*, 237–271.

Hilberg, S., & Kreuzer, M. (2013). Identification of a deep flow system in a dolomitic alpine aquifer–Case study Wimmerbauern spring, Bad Ischl. *Austria Journal of Earth Sciences*, *106*, 16–25.

Hornberger, G. M., & Spear, R. C. (1981). Approach to the preliminary analysis of environmental systems. *Journal of Environmental Management*, *12*, 7–18.

Kaufmann, G., & Braun, J. (2001). Modelling karst denudation on a synthetic landscape. *Terra Nova*, *13*, 313–320.

Kralik, M. (2001). Strategie zum Schutz der Karstwassergebiete in Österreich. Teil 1: Problemanalyse in Form der Auswertung einer Fragebogenaktion; Teil 2. In *Karstwasserfakten und praktisch-wissensch aftliche Problemlösungsvorschläge* (p. 189). Umweltbundesamt.

Kunaver, J. (1979). Some experiences in measuring the surface karst denudation in high-alpine environment, Actes du symposium international sur l'erosion karstique, UIS, Commision de erosion du karst, Aix-en-Provence-Marseille-Nimes, pp. 75–85.

Linan Baena, C., Andreo, J., Mudry, J., Carrasco, F., & Cantos, F. (2009). Groundwater temperature and electric conductivity as tools to characterize flow patterns in carbonate aquifers; sierra de las Nieves karst aquifer, southern Spain. *Hydrogeology Journal*, *17*, 843–853.

Liu, Z., & Zhao, J. (1999). Contribution of carbonate rock weathering to the atmospheric CO_2 sink. *Environmental Geology*, *39*, 1053–1058.

Loncar, G., Sreng, Z., Bekic, D., & Kunstek, D. (2018). Hydraulic-hydrology analysis of the turbulent seepage flow within karst aquifer of the Golubinka spring catchment. *Hindawi Geofluids*, *2018*, 12.

Martin, J. B., & Dean, R. W. (2001). Exchange of water between conduits and matrix in the Floridan aquifer. *Chemical Geology*, *179*, 145–165.

Mazzilli, N., Guinot, V., Jourde, H., Lecoq, N., Labat, D., Arfib, B., … Bertin, D. (2017). KarstMod: A modelling platform for rainfall-discharge analysis and modelling dedicated to karst systems. *Environmental Modelling & Software*, *122*, 1–7.

Mudarra, M., & Andreo, B. (2010). Hydrogeological functioning of a karst aquifer deduced from hydrochemical components and natural organic

tracers present in spring waters. The case of Yedra spring (southern Spain). *Acta Carsologica*, *39*, 261–270.

Nash, J. E., & Sutcliffe, J. (1970). River flow forecasting through conceptual models: Part 1a discussion of principles. *Journal of Hydrology*, *10*, 282–290.

Petalas, C. P., Akratos, C. S., & Tsihrintzis, V. A. (2018). Hydrogeological investigation of a karst aquifer system. *Environmental Processes*, *5*, 155–181.

Plan, L. (2005). Factors controlling carbonate dissolution rates quantified in a field test in the Austrian Alps. *Geomorphology*, *68*, 201–212.

Poulain, A., Watlet, A., Kaufmann, O., Van Camp, M., Jourde, H., Mazzilli, N., … Hallet, V. (2018). Assessment of groundwater recharge processes through karst vadose zone by cave percolation monitoring. *Hydrological Processes*, *32*, 2069–2083.

Pronk, M., Goldscheider, N., & Zopfi, J. (2007). Particle-size distribution as indicator for fecal bacteria contamination of drinking water from karst springs. *Environmental Science & Technology*, *41*, 8400–8405.

Ravbar, N., Engelhardt, I., & Goldscheider, N. (2011). Anomalous behaviour of specific electrical conductivity at a karst spring induced by variable catchment boundaries: The case of the Podstenjsek spring, Slovenia. *Hydrological Processes*, *25*, 2130–2140.

Rössler, O., Diekkrüger, B., & Löffler, L. (2012). Potential drought stress in a Swiss mountain catchment–Ensemble forecasting of high mountain soil moisture reveals a drastic decrease, despite major uncertainties. *Water Resources Research*, *48*, 1–19.

Saltelli, A. (2002). Making the best use of model evaluations to compute sensitivity indices. *Computer Physics Communications*, *145*, 280–297.

Saltelli, A., Ratto, M., Andres, T., Campolongo, F., Cariboni, J., Gatelli, D., … Tarantola, S. (2008). *Global sensitivity analysis: The primer*. John Wiley & Sons Ltd.

Sivelle, V., Labat, D., Mazzilli, N., Massei, N., & Jourde, H. (2019). Dynamics of the flow exchanges between matrix and conduits in Karstified watersheds at multiple temporal scales. *Water*, *11*, 569.

Sobol, I. M. (1977). Uniformly distributed sequences with an additional uniform property. *USSR Computational Mathematics and Mathematical Physics*, *16*, 236–242.

Stevanović, Z. (2018). Global distribution and use of water from karst aquifers. In M. Parise, F. Gabrovsek, G. Kaufmann, & N. Ravbar (Eds.), *Advances in karst research: Theory, fieldwork and applications* (Vol. 466, pp. 217–236). Geological Society of London, Special Publications.

Vigna, B., & Banzato, C. (2015). The hydrogeology of high-mountain carbonate areas: An example of some alpine systems in southern Piedmont (Italy). *Environmental Earth Sciences*, *74*, 267–280.

Werner, R. (2007). *Klima von Vorarlberg* (Vol. 2). Amt der Vorarlberg Landesregierung.

White, W. B. (1984). Rate processes: Chemical kinetics and karst landform development. In L. Fleur (Ed.), *Groundwater as a geomorphic agent*. Allen and Unwin.

Yoshimura K., & Inukura Y. (1997). The geochemical cycle of carbon dioxide in a carbonate rock area, Akiyoshi-dai Plateau, Yamaguchi, Southwestern Japan, proc. 30th Int'l. Geol. 24. pp. 114–126.

Zeng, C., Gremaud, V., Zeng, H., Liu, Z., & Goldscheider, N. (2012). Temperature-driven meltwater production and hydrochemical variations at a glaciated alpine karst aquifer: Implication for the atmospheric CO_2 sink under global warming. *Environmental Earth Sciences*, *65*, 2285–2297.

How to cite this article: Frank S, Goeppert N, Goldscheider N. Improved understanding of dynamic water and mass budgets of high-alpine karst systems obtained from studying a well-defined catchment area. *Hydrological Processes*. 2021;35: e14033. https://doi.org/10.1002/hyp.14033